THE JOURNAL OF PHYSICAL CHEMISTRY A LETTERS

2007, *111,* 544−548
Published on Web 01/04/2007

A Spectroscopic Study of Atmospherically Relevant Concentrated Aqueous Nitrate Solutions

Paula K. Hudson,[†,‡] Jaclyn Schwarz,[†] Jonas Baltrusaitis,[†] Elizabeth R. Gibson,[†] and Vicki H. Grassian*[,†,‡]

Department of Chemistry and the Center for Global and Regional Environmental Research, The University of Iowa, Iowa City, Iowa 52242

Received: September 29, 2006; In Final Form: November 28, 2006

Concentrated aqueous nitrate aerosols are present in the Earth's atmosphere as a result of heterogeneous reactions of sea salt and mineral dust aerosol with nitrogen oxides (e.g., NO_2, NO_3, HNO_3 and N_2O_5). Because the water content of these aerosols depends on relative humidity (RH), the composition and nitrate ion concentration will also depend on RH. Unlike the original aerosols, aqueous nitrate aerosols are photochemically active at solar wavelengths. To gain a better understanding of the nitrate ion chromophore in concentrated aqueous nitrate aerosols, we have measured the ATR-FTIR and UV/vis spectra of concentrated nitrate solutions over a large concentration range. Both ATR-FTIR and UV/vis spectroscopy show changes in the nitrate ion spectra with increasing concentration. Ab initio calculations are used to aid in the assignment and interpretation of these spectra. From these data, we predict that the photoreactivity of aqueous nitrate aerosols will strongly depend on relative humidity as the molecular and electronic structure of the nitrate ion becomes increasingly perturbed from that of the isolated ion in highly concentrated atmospherically relevant solutions.

Introduction

As sea salt and mineral dust are transported in the atmosphere, these aerosol can undergo heterogeneous chemistry with gas-phase nitrogen oxides.[1,2] These reactions typically result in the formation of particulate and adsorbed nitrates. Infrared spectroscopy has shown that reactions of iron and aluminum oxides with HNO_3 result in the formation of adsorbed nitrate.[3,4] For the carbonate component of mineral dust aerosol, heterogeneous reactions with nitrogen oxides convert solid carbonate particles into aqueous nitrate solutions.[5] For example, it has been shown that reaction of calcite ($CaCO_3$) and dolomite ($CaMg(CO_3)_2$) with nitric acid results in aqueous calcium nitrate aerosol and a 1:1 mixture of aqueous calcium nitrate and magnesium nitrate aerosol, respectively, according to the following reactions:[6,7]

$$CaCO_3(s) + 2HNO_3(g) \xrightarrow{\%\ RH} Ca(NO_3)_2(s, aq) + CO_2(g) + H_2O \quad (1)$$

$$CaMg(CO_3)_2(s) + 4HNO_3(g) \xrightarrow{\%\ RH} Ca(NO_3)_2(s, aq) + Mg(NO_3)_2(s, aq) + 2CO_2(g) + 2H_2O \quad (2)$$

The importance of the above reactions in terms of the implications of converting solid particles into aqueous aerosol in the atmosphere has already been discussed in some detail.[8,9] For the aqueous aerosol, both the composition and size of the aerosol depend on relative humidity (RH). The hygroscopic growth of the aerosol with increasing RH increases the amount of light scattering in the infrared due to the larger size of the aerosol. In addition, the aqueous aerosol is a much more effective cloud condensation nucleus.

Here we consider the photoreactivity of the nitrate aerosol and, in particular, the potential changes as a function of relative humidity. Solar radiation reaching the Earth's surface is attenuated by atmospheric constituents that absorb and scatter solar light. There is a steep cutoff in the solar spectral distribution reaching the Earth's surface beginning near 320 nm as it approaches shorter wavelengths. Radiation below 290 nm is completely absorbed by stratospheric ozone (O_3) and does not reach the Earth's surface.[10] Photolysis of aqueous nitrate at $\lambda > 290$ nm and pH < 6 proceeds via two major channels:[11−17]

$$NO_3^- + H^+ \xrightarrow{h\nu} NO_2 + {}^{\bullet}OH \quad (3)$$

$$NO_3^- \xrightarrow{h\nu} NO_2^- + O(^3P) \quad (4)$$

Nitrate ions are an important chromophore in natural waters and play a crucial role in the chemistry of snowpacks, acting as a source of NO_x and OH radicals.[18−22] Additionally, the resulting OH radical and $O(^3P)$ that are formed are highly reactive in both the gas and aqueous phase.[10,23]

In this Letter, we focus on spectroscopic studies of concentrated calcium nitrate solutions, an atmospherically relevant reaction product of mineral dust aerosol and nitrogen oxides, using attenuated total reflectance Fourier transform infrared (ATR-FTIR) spectroscopy and ultraviolet/visible (UV/vis) spectroscopy. Ab initio calculations of the isolated nitrate ion and a nitrate ion in a water cluster provide important insights

* To whom correspondence should be addressed. E-mail: vicki-grassian@uiowa.edu. Tel: 319-335-1392. Fax: 319-353-1115.
[†] Department of Chemitry.
[‡] Center for Global and Regional Environmental Research.

10.1021/jp0664216 CCC: $37.00

into these spectroscopic measurements and their atmospheric implications.

Experimental Methods

Spectroscopic Methods. ATR-FTIR spectroscopy was used to measure the vibrational spectrum from 750 to 4000 cm^{-1} at 4 cm^{-1} resolution co-adding 150 scans of calcium nitrate ($Ca(NO_3)_2$) solutions over a range of concentrations. These spectra were referenced to pure water. These measurements were done using a horizontal liquid cell with a zinc selenide (ZnSe) internal reflection element (Pike Technology). UV/vis spectroscopy (Perkin-Elmer, Lambda 20 UV/vis spectrometer) was used to measure the absorption maximum of the $n-\pi^*$ transition over 4 orders of magnitude in $Ca(NO_3)_2$ solution concentration. UV/vis quartz cuvettes with 1 cm (Light Path Cells, Inc.), 1 mm (NSG Precision Cells, Inc.), and 0.1 mm (Perkin-Elmer) pathlengths were used to acquire absorption spectra over this large concentration range. The focus of this study is on calcium nitrate solutions; however, several experiments using other nitrate salts were also performed.

Ab Initio Calculations. Ab initio calculations for the free NO_3^- ion and the $Ca(NO_3)^+ \cdot 10H_2O$ cluster were performed using Spartan '04 (version 1.0.3).[24] Energy optimization and vibrational frequency calculations were both done using the B3LYP hybrid density functional theory (DFT) level of theory with a 6-31+G(d) basis set. To account for anharmonicity in the calculated vibrational frequencies, a scaling factor of 0.9632, reported for the B3LYP/6-31+G(d, p) basis set, was used.[25] As discussed previously, the value of the scaling factor depends weakly upon the basis set for a given level of theory.[26] Optimized structures were determined without symmetry constraints on any of the molecules. Stationary points were identified as true minima of the potential energy surface (PES) in all cases because no imaginary frequencies were found.

Source of Chemicals and Solution Preparation. $Ca(NO_3)_2$ solutions were made from a number of stock solutions ranging in concentration from 0.02 to 15.4 molality (*m*) (nitrate ion concentrations range from 0.04 to 30.8 *m*) using calcium nitrate tetrahydrate ($Ca(NO_3)_2 \cdot 4H_20$, Alfa Aesar, CAS# 13477-34-4, ACS 99.0−103.0%) and Optima water (Fisher Scientific, W7-4). The $Ca(NO_3)_2$ stock solutions were diluted resulting in solutions with concentrations ranging from 0.008 to 15.4 *m* (0.016−30.8 *m* NO_3^-) for UV/vis measurements and 0.06 to 15.2 *m* (0.012−30.4 *m* NO_3^-) for ATR-FTIR measurements. $NaNO_3$ (Sigma-Aldrich, CAS# 7631-99-4, ACS) and $Mg(NO_3)_2 \cdot 6H_20$ (Alfa Aesar, CAS# 13446-18-9, ACS 98.0−102.0%), and the 1:1 $Ca(NO_3)_2$:$Mg(NO_3)_2$ solutions were made in a similar manner.

Results and Discussion

Aqueous Calcium Nitrate Aerosols: Water Content as a f(RH). In a previous study, we reported on the hygroscopic growth of 100 nm size-selected $Ca(NO_3)_2$ particles as a function of relative humidity using a tandem differential mobility analyzer.[9] From the hygroscopic growth curve, the water content of the nitrate aerosol can be calculated using Köhler theory. The results are plotted in Figure 1a in terms of the water to solute ratio (WSR) and in Figure 1b in terms of the nitrate ion concentration (*m*) of the aerosol. These data show that aqueous calcium nitrate aerosols are highly concentrated under atmospherically relevant conditions. Near 15% RH, the concentration of nitrate in the aerosol is 40 *m* and decreases by an order of magnitude to 4 *m* near 90% RH.

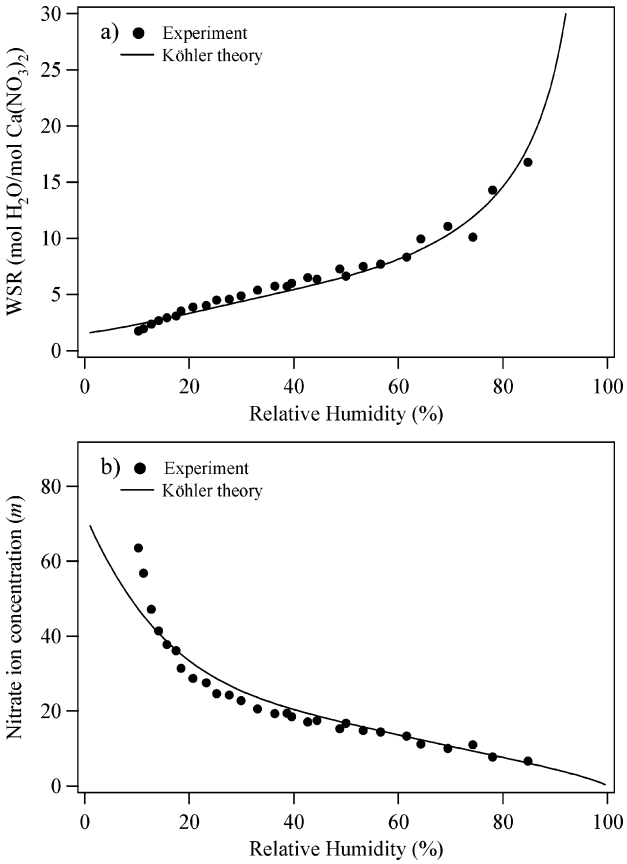

Figure 1. (a) Water to solute ratio and (b) nitrate concentrations as a function of RH calculated for 100 nm particles. The filled circles are the experimental data and the solid line is the calculated curve based on Köhler theory. The experimental data are in good agreement with Köhler theory above 50% RH but deviate for the more concentrated solutions below 50% RH. The data used in this figure are obtained using a tandem differential mobility analyzer discussed in detail in ref 9.

It is expected that the molecular and electronic structure of the nitrate ion will be perturbed in these highly concentrated solutions.[27−29] To better understand the structure of the nitrate ion in concentrated aqueous calcium nitrate aerosol, a spectroscopic study was carried out on concentrated aqueous calcium nitrate solutions. The results of a combined study using ATR-FTIR and UV/vis spectroscopy along with ab initio calculations of aqueous-phase solutions of atmospherically relevant concentrations are presented below.

Spectroscopic Investigation of Aqueous Calcium Nitrate Solutions and Ab Initio Calculations of Nitrate and Nitrate Water Clusters. In the gas phase, the nitrate ion is planar with D_{3h} symmetry. Ab initio calculations of the infrared spectrum of the isolated nitrate ion and a cluster containing a nitrate ion, calcium ion, and ten water molecules in the spectral range extending from 700 to 1550 cm^{-1} is shown in Figure 2. For the isolated nitrate ion, the most intense band in the spectrum of Figure 2a is seen at 1351 cm^{-1} (ν_3, asymmetric stretch) and a much weaker band is seen at 796 cm^{-1} (ν_2, out-of-plane deformation). The infrared assignment and the calculated bond angles, bond lengths and molecule planarity for the isolated nitrate ion are given in Table 1. As has been previously shown, the experimental spectrum of the aqueous nitrate ion is more complicated than the calculated isolated ion spectrum. The ATR-FTIR spectra of aqueous $Ca(NO_3)_2$ as a function of increasing solution concentration are shown in Figure 3. A comparison of the experimental spectra to the calculated gas-phase nitrate

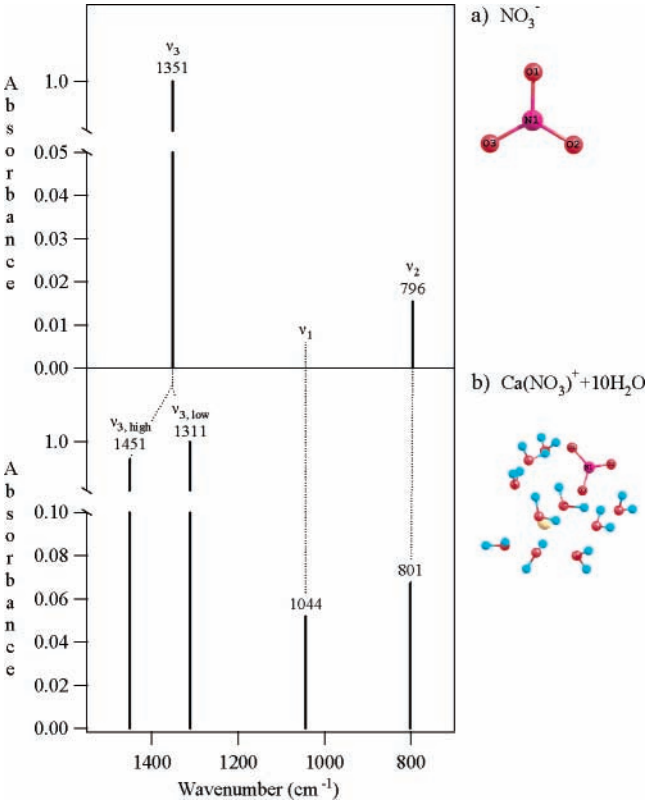

Figure 2. Stick representation of the calculated infrared spectrum of (a) an isolated nitrate ion and (b) a cluster containing a calcium ion, nitrate ion and ten water molecules. The calculations of the molecule configurations are displayed to the right of each respective panel. It can be seen from the calculations that the nitrate ν_3 degenerate mode splits and the ν_1 symmetric stretch becomes infrared active in the cluster.

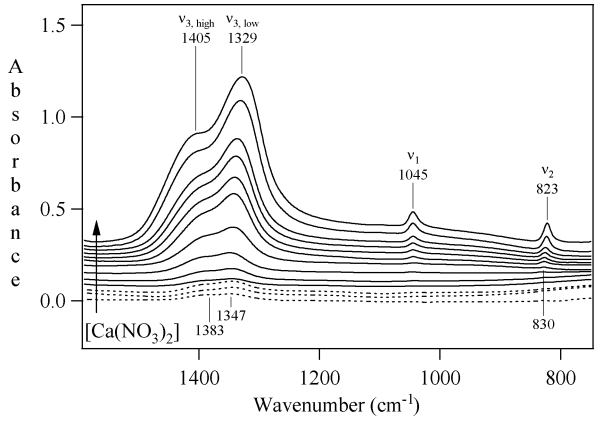

Figure 3. ATR-FTIR spectra of calcium nitrate solutions ranging from 0.06 to 15.2 *m* (0.12−30.4 *m* NO_3^-). The three lowest concentration spectra (dotted lines) have been multiplied by a factor of 4, 2, and 2, respectively. The splitting of the ν_3 degenerate mode into two bands labeled $\nu_{3,high}$ and $\nu_{3,low}$ increases with increasing concentration. The ν_1 and ν_2 symmetric stretches become visible near 1.6 *m* NO_3^- at 1045 and 830 cm^{-1}, respectively. The frequency of the ν_2 symmetric stretch decreases with increasing concentration. All spectra have been offset for clarity.

spectrum shows several differences. First, the singleton at 1351 cm^{-1} in the gas-phase spectrum now consists of at least two peaks with relative intensities that vary as a function of concentration. Additionally, the frequency difference between the two peaks increases with increasing concentration. Similar splitting and increased intensity of the ν_3 peak has been observed in the infrared and Raman spectra of concentrated $Ca(NO_3)_2$[27] and concentrated $Mg(NO_3)_2$ solutions.[30,31] Second, the ν_1 vibrational mode, inactive for the isolated nitrate ion, is observed in the solution-phase spectrum at 1045 cm^{-1}. The appearance of this band has been previously reported in other infrared studies of aqueous nitrate solutions.[27] Third, the ν_2 out-of-plane deformation mode at 830 cm^{-1} at a nitrate ion concentration of ca. 1.6 *m* shifts to lower wavenumbers with increasing concentration.

To better understand these solution-phase data beyond the symmetry discussion posed in previous work,[27] ab initio calculations of a cluster containing a nitrate ion, calcium ion and ten water molecules were performed. As shown in Figure 2b, the nitrate ion in the cluster compound has two peaks in the ν_3 region at 1451 and 1311 cm^{-1}. Furthermore, the ν_1 mode at 1044 cm^{-1} becomes infrared active. This infrared absorption band is of nearly equal intensity to the ν_2 mode at 801 cm^{-1}. This is in agreement with the measured ATR-FTIR spectrum (Figure 3) which also shows similar intensities of the ν_1 and ν_2 modes.

The calculated N−O bond lengths and bond angles of the energy minimized nitrate ion and with Ca^{2+} in the water cluster are given in Table 1. Comparison of the structure of the free nitrate and the nitrate in the cluster shows: (i) the N−O bond lengths are different and no longer equivalent in the water cluster calculation; (ii) the O−N−O bond angles are also no longer equivalent in the water cluster; and (iii) the nitrate ion is slightly less planar in the water cluster. In accord with previous measurements and calculations, the symmetry of the NO_3 ion is lowered in the presence of solvent molecules and a counter ion.[27,29,32]

The asymmetry in the N−O bond lengths is important from the perspective of the electronic structure as a nonsymmetric and slightly nonplanar structure should result in a decrease in conjugation. Furthermore, the $\pi-\pi^*$ and $n-\pi^*$ transitions will increase in energy with the corresponding loss of symmetry and planarity. UV/vis spectroscopy can be used to probe these transitions in concentrated nitrate salt solutions.

Figure 4 shows measured UV/vis spectra for calcium nitrate solutions over a molality range spanning four orders of magnitude. Figure 4 is plotted with respect to molality and replotted with respect to molarity (M) in the Supporting Information (Figure S1). The spectra are specifically shown in the region of the $n-\pi^*$ transition. All of the spectra plotted in Figure 4a have been normalized to unity such that the absorbance at the absorption maximum near 300 nm was set equal to one. The color image plot shown provides insight into the change in the

TABLE 1: Ab Initio Calculations for the Isolated Nitrate Ion and the Calcium Nitrate Ion Cluster

structure	frequency (cm^{-1})	bond lengths (Å)		bond angles (deg)		planarity (deg)
NO_3^-	1351 (ν_3)	N1−O1	1.27	O1−N1−O2	120	180
	796 (ν_2)	N1−O2	1.27	O1−N1−O3	120	
		N1−O3	1.27	O2−N1−O3	120	
$Ca(NO_3)^+ \bullet 10H_2O$	1451 ($\nu_{3,high}$)	N1−O1	1.27	O1−N1−O2	121.2	179.3
	1311 ($\nu_{3,low}$)	N1−O2	1.23	O1−N1−O3	118.3	
	1044 (ν_1)	N1−O3	1.28	O2−N1−O3	120.5	
	801 (ν_2)	Ca−O3	2.55			

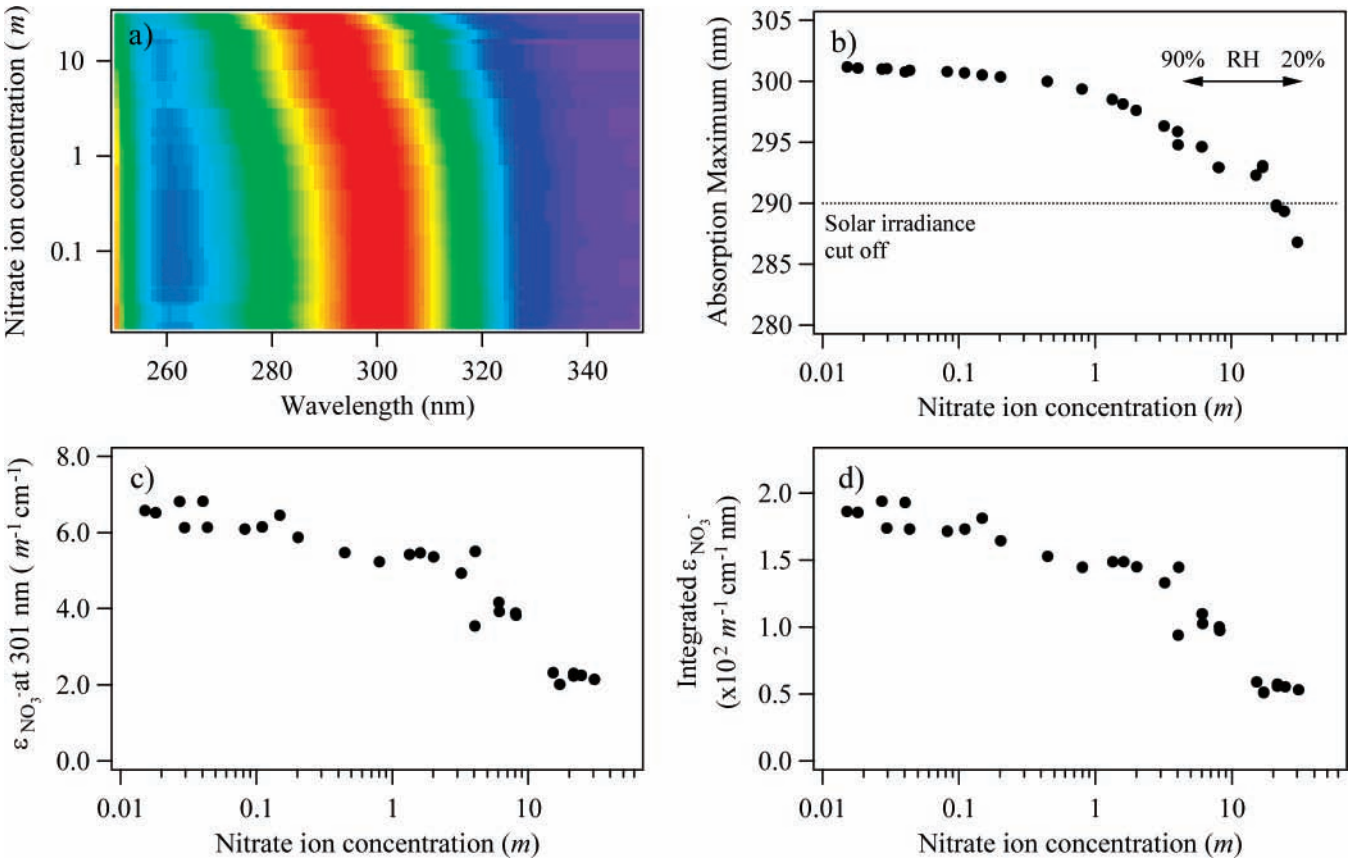

Figure 4. (a) Plot of UV/vis spectra of calcium nitrate solutions from 0.016 to 30.8 *m* NO_3^-. For each concentration, the peak intensity has been normalized to unity (red = 1, purple = 0) to more clearly show the shift in the absorption band maximum as a function of NO_3^- concentration. (b) Absorbance maximum (nm) as a function of NO_3^- concentration (log *x* scale). It is seen that the absorption maximum shifts from a value of 301 nm to shorter wavelengths, reaching 287 nm at 30.8 *m*. The region from ca. 4−34 *m* corresponds to 90−20% RH, respectively. (c) Molal absorptivity (m^{-1} cm^{-1}) at a wavelength of 301 nm as a function of NO_3^- concentration. The molal absorptivity is nearly constant at NO_3^- concentrations less than 0.2 *m* with a value of 6.4 ± 0.1 m^{-1} cm^{-1}; it then decreases steadily until 8 *m* NO_3^-. Above this concentration it decreases more rapidly. (d) Integrated molal absorptivity (m^{-1} cm^{-1} nm) from 290−350 nm as a function of NO_3^- concentration. Similar results are observed as with (c).

absorption maximum with increasing solution-phase concentration. The data show that below a nitrate ion concentration of ca. 0.4 *m*, the absorption maximum is nearly constant with a value of 301 nm and an absorption onset, defined as the wavelength at which linear extrapolations of the initially steeply rising portion of the absorption spectrum and the background absorbance intersect,[33] at 362 nm. Above 0.4 *m* NO_3^-, the absorption maximum begins to decrease in wavelength and the data show that there is a nonlinear decrease in the wavelength maximum as a function of increasing nitrate ion concentration. The peak maximum decreases to 287 nm at 30.8 *m* NO_3^- with an absorption onset at 349 nm. The consistency in the width of the absorption peak is evident visually in the color band in Figure 4a as well as numerically by the absorption onset. Figure 4b shows the peak absorbance wavelength as a function of NO_3^- concentration. The region of atmospherically relevant concentrations highlighted by the arrow from 90 to 20% RH, 4−34 *m*, shows a large degree of change in absorption maximum ranging from 295 to 287 nm, respectively. Additional experiments with $NaNO_3$, $Mg(NO_3)_2$, and a 1:1 molar mixture of $Ca(NO_3)_2$ and $Mg(NO_3)_2$ also show a shift in the n−π* absorption maximum for each of these solutions. For $Mg(NO_3)_2$ and $NaNO_3$ there is a shift from 2 to 4 nm up to 10 *m* in nitrate ion concentration and the mixture has nearly a 10 nm shift up to 20 *m* in nitrate ion concentration.

The shift in the UV/vis absorption maximum is of particular importance for the resulting photochemical activity of the nitrate aerosols as solar radiation at wavelengths less than 290 nm does not reach the Earth's surface. This suggests that the more concentrated aerosol, at lower relative humidity, will not be as photochemically active as the more dilute aerosol.

To emphasize this point, Figure 4c shows the molal absorptivity (m^{-1} cm^{-1}) as a function of nitrate concentration at 301 nm. The maximum molal absorptivity occurs at nitrate ion concentrations less than 0.1 *m* with an average value of 6.4 ± 0.01 m^{-1} cm^{-1}. This is in close agreement with previous reports for molar absorptivities of $NaNO_3$ and nitrate ion.[12,23] (See the Supporting Information (Figure S1c) for the molar absorptivity calculation.) At nitrate concentrations greater than 0.1 *m* the molal absorptivity decreases steadily until 8 *m* NO_3^-. Above this concentration the change in molal absorptivity as a function of concentration is much sharper. As shown in Figure 4d, similar results are found for the integrated molal absorptivity when integrated with respect to atmospherically relevant wavelengths (>290 nm).

Conclusions and Atmospheric Implications

We have correlated spectral changes observed in atmospherically relevant concentrations of aqueous nitrate solutions with potential changes in the photochemical activity of nitrate aerosols as a function of relative humidity. We show that for atmospherically relevant concentrated solutions of $Ca(NO_3)_2$, the nitrate ion becomes less planar and the N−O bond lengths are no longer equivalent resulting in a lower symmetry than D_{3h} for this molecular ion. This distortion leads to vibrational transitions which become infrared active and shift the n−π*

transition to higher energies. Furthermore, the combined data from Figure 4 show that at atmospherically relevant concentrations (between 4 and 40 *m*), the n−π* absorption shifts to higher energies with higher concentrations and there is a large decrease in the molal absorptivity. Because the n−π* transition is close to the solar spectrum cut off of 290 nm, the change in absorptivity of the nitrate ion with RH has potentially important ramifications for the photochemical activity of nitrate aerosols and the photochemical production of nitrite and O−H radicals in these aerosols.

Acknowledgment. This material is based upon work supported by the National Science Foundation under Grant No. 0503854. Any opinions, findings, and conclusions or recommendations expressed in this material are those of the authors and do not necessarily reflect the views of the National Science Foundation.

Supporting Information Available: Description of how molarity is determined from molality in addition to a remake of Figure 4 shown in units of molarity. This material is available free of charge via the Internet at http://pubs.acs.org.

References and Notes

(1) Finlayson-Pitts, B. J. *Chem. Rev.* **2003**, *103*, 4801.

(2) Grassian, V. H. *Int. Rev. Phys. Chem.* **2001**, *20*, 467.

(3) Frinak, E. K.; Wermeille, S. J.; Mashburn, C. D.; Tolbert, M. A.; Pursell, C. J. *J. Phys. Chem. A* **2004**, *108*, 1560.

(4) Goodman, A. L.; Underwood, G. M.; Grassian, V. H. *J. Geophys. Res.* **2000**, *105*, 29053.

(5) Krueger, B. J.; Grassian, V. H.; Laskin, A.; Cowin, J. P. *Geophys. Res. Lett.* **2003**, *30*, *1148*, doi: 10.1029/2002GL016563.

(6) Krueger, B. J.; Grassian, V. H.; Cowin, J. P.; Laskin, A. *Atmos. Environ.* **2005**, *39*, 395.

(7) Krueger, B. J.; Grassian, V. H.; Cowin, J. P.; Laskin, A. *Atmos. Environ.* **2004**, *38*, 6253.

(8) Gibson, E. R.; Hudson, P. K.; Grassian, V. H. *Geophys. Res. Lett.* **2006**, *33*, *L13811*, doi: 10.1029/2006GL026386.

(9) Gibson, E. R.; Hudson, P. K.; Grassian, V. H. *J. Phys. Chem. A* **2006**, *110*, 11785.

(10) Seinfeld, J. H.; Pandis, S. *Atmospheric Chemistry and Physics: From Air Pollution to Climate Change*; John Wiley & Sons, Inc.: New York, 1998.

(11) Boxe, C. S.; Colussi, A. J.; Hoffmann, M. R.; Murphy, J. G.; Wooldridge, P. J.; Bertram, T. H.; Cohen, R. C. *J. Phys. Chem. A* **2005**, *109*, 8520.

(12) Chu, L.; Anastasio, C. *J. Phys. Chem. A* **2003**, *107*, 9594.

(13) Dubowski, Y.; Colussi, A. J.; Hoffmann, M. R. *J. Phys. Chem. A* **2001**, *105*, 4928.

(14) Mack, J.; Bolton, J. R. *J. Photochem. Photobiol. A* **1999**, *128*, 1.

(15) Mark, G.; Korth, H.-G.; Schuchmann, H.-P.; von Sonntag, C. *J. Photochem. Photobiol. A* **1996**, *101*, 89.

(16) Warneck, P.; Wurzinger, C. *J. Phys. Chem.* **1988**, *92*, 6278.

(17) Zellner, R.; Exner, M.; Herrmann, H. *J. Atmos. Chem.* **1990**, *10*, 411.

(18) Beine, H. J.; Domine, F.; Ianniello, A.; Nardino, M.; Allegrini, I.; Teinila, K.; Hillamo, R. *Atmos. Chem. Phys.* **2003**, *3*, 335.

(19) Davis, D.; Nowak, J. B.; Chen, G.; Buhr, M.; Arimoto, R.; Hogan, A.; Eisele, F.; Mauldin, L.; Tanner, D.; Shetter, R.; Lefer, B.; McMurry, P. *Geophys. Res. Lett.* **2001**, *28*, 3625.

(20) Honrath, R. E.; Peterson, M. C.; Guo, S.; Dibb, J. E.; Shepson, P. B.; Campbell, B. *Geophys. Res. Lett.* **1999**, *26*, 695.

(21) Ridley, B.; Walega, J.; Montzka, D.; Grahek, F.; Atlas, E.; Flocke, F.; Stroud, V.; Deary, J.; Gallant, A.; Boudries, H.; Bottenheim, J.; Anlauf, K.; Worthy, D.; Sumner, A. L.; Splawn, B.; Shepson, P. *J. Atmos. Chem.* **2000**, *36*, 1.

(22) Young, M. A. Environmental Photochemistry in Surface Waters. In *Water Encyclopedia: Oceanography; Meteorology; Physics and Chemistry; Water Law; and Water History, Art, and Culture*; Lehr, J. H., Keeley, J., Eds.; John Wiley and Sons, Inc.: New York, 2005.

(23) *Environmental Photochemistry Part II*; Boule, P., Bahnemann, D. W., Roberston, P. K. J., Eds.; Springer: Berlin, 2005; Vol. 2, pp 489.

(24) Kong, J.; White, C. A.; Krylov, A. I.; Sherrill, D.; Adamson, R. D.; Furlani, T. R.; Lee, M. S.; Lee, A. M.; Gwaltney, S. R.; Adams, T. R.; Ochsenfeld, C.; Gilbert, A. T. B.; Kedziora, G. S.; Rassolov, V. A.; Maurice, D. R.; Nair, N.; Shao, Y. H.; Besley, N. A.; Maslen, P. E.; Dombroski, J. P.; Daschel, H.; Zhang, W. M.; Korambath, P. P.; Baker, J.; Byrd, E. F. C.; Van Voorhis, T.; Oumi, M.; Hirata, S.; Hsu, C. P.; Ishikawa, N.; Florian, J.; Warshel, A.; Johnson, B. G.; Gill, P. M. W.; Head-Gordon, M.; Pople, J. A. *J. Comput. Chem.* **2000**, *21*, 1532

(25) Irikura, K. K.; Johnson, R. D.; Kacker, R. N. *J. Phys. Chem. A* **2005**, *109*, 8430.

(26) Wong, M. W. *Chem. Phys. Lett.* **1996**, *256*, 391

(27) Irish, D. E.; Walrafen, G. E. *J. Chem. Phys.* **1967**, *46*, 378.

(28) Waterland, M. R.; Kelley, A. M. *J. Chem. Phys.* **2000**, *113*, 6760.

(29) Waterland, M. R.; Stockwell, D.; Kelley, A. M. *J. Chem. Phys.* **2001**, *114*, 6249.

(30) Zhang, Y. H.; Choi, M. Y.; Chan, C. K. *J. Phys. Chem. A* **2006**, *110*, 7516.

(31) Zhang, Y. H.; Choi, M. Y.; Chan, C. K. *J. Phys. Chem. A* **2004**, *108*, 1712.

(32) Ahlijah, G. E. B. Y.; Mooney, E. F. *Spectrochim. Acta Part A* **1969**, *25*, 619.

(33) Urquhart, R. S.; Furlong, D. N.; Mansur, H.; Grieser, F.; Tanaka, K.; Okahata, Y. *Langmuir* **1994**, *10*, 899.